SWIFT-XRT-CALDB-04

CALDB Version: 20200724

Release Date: 2020-Aug-11

Prepared by: Andrew Beardmore, Kim Page (UL), Matteo Perri, Milvia Capalbi (ASDC)

Date revised: 2020-Oct-01

Revision: 21

Revised by: Andrew Beardmore

SWIFT-XRT CALDB RELEASE NOTE

SWIFT-XRT-CALDB-04: Gain

1 Component Files

Table 1: CALDB gain files issued since last release note.

FILENAME[a]	VALID DATE[b]	RELEASE DATE[c]	REVISION[d]
swxpcgains6_20010101v020.fits	2001-Jan-01	2020-Aug-11	21
swxwtgains6_20010101v022.fits	2001-Jan-01	2020-Aug-11	21

[a]Filenames containing the characters **'s0'** refer to substrate voltage (V_{ss}) 0 V gain files, while **'s6'** refer to V_{ss} = 6 V gain files; the substrate voltage was raised permanently to 6V on 2007-Aug-30 at 14:25UT. **'v0XX'** is the version of the gain file for the particular readout mode ('pc' − Photon Counting; 'wt' − Windowed Timing; 'pd' − Photo-Diode), substrate voltage and epoch.

[b]Date from which the file is first used.

[c]HEASARC CALDB release date.

[d]Release revision number.

2 Introduction

This document describes updates to the *Swift*/XRT Calibration Database (CALDB) gain files made since the 2019-Oct-23 release (previously discussed in release note SWIFT-XRT-CALDB-04_v20).

This is an incremental release, providing updated gain coefficients and trap depth estimates from 2019-Jun-01 to 2020-May-30 for both the Photon Counting (PC) and Windowed Timing (WT) mode gain files, following the procedures outlined in SWIFT-XRT-CALDB-04_v20.

This document is structured as followed. Section 3 provides a summary of the updates which have gone into the gain files issued in this release. Section 4 discusses known limitations with the gain calibration. Appendix A illustrates the derivation behind the gain and CTI coefficients and their implementation in the CALDB gain files. Appendix B describes the gain and CTI measurements, while the charge trap analysis details are given in Appendix C. Appendix D lists the previous gain file releases.

3 Updates to the Gain Files

Radiation damage causes degradation to the CCD spectral response due to the build up of charge trapping sites in the silicon crystalline structure of the detector, which retain charge, resulting in incomplete X-ray event energy reconstruction. Updates to the gain and CTI coefficients (Section B), as well as the charge trap-correction offsets table (Section C), help maintain the accuracy of the gain corrected energy scale and partially recover the spectral resolution.

3.1 New Release (Revision 21) Summary

Observations of the Tycho and Cas A supernova remnants are scheduled once a year to monitor the evolution of the spectral response of the CCD using their strong Si-Kα lines. The observing strategy employed to acquire the trap calibration data was the same as that used for the previous releases (see release note SWIFT-XRT-CALDB-04_v18 and references therein) and is described in Section C. For Photon Counting (PC) mode, 15×20ks observations of the Tycho SNR were obtained from 2019 August – December, spread over the entire CCD, but with the greatest exposure covering the central 200×400 pixels (where the majority of XRT observations are performed). For Windowed Timing (WT) mode, 6×10ks observations of Cas A were taken during 2019 September, covering the central 200×300 pixels.

An idea of the uncertainties in the energy scale reconstruction approximately one year after the release of the gain files can be obtained by processing the new data with the gain files from the previous CALDB release. For example, when the latest PC mode Tycho observations are processed with the previous version of the PC gain file (i.e. v019, swxpcgains6_20010101v019.fits), energy shifts of the silicon [iron] emission lines of $\sim$ 25 [75] eV are seen with respect to the expected reference values when averaged over the entire CCD. Similarly, when the WT mode Cas A data are processed with the previous version of the WT gain file (v021, swxwtgains6_20010101v021.fits), energy shifts of the silicon [iron] emission lines of $\sim$ 50 [120] eV are seen over the central 200 rows of the CCD.

To restore the accuracy of the gain corrected energy scale, incrementally updated versions of the PC and WT gain files have been generated and are included in this release as files **swxpcgains6_20010101v020.fits** and **swxwtgains6_20010101v022.fits**, respectively. The updates include:

- New gain and CTI coefficients derived from analysis of the corner source data collected from 2019 June to 2020 May (see Section B). The coefficients invoked when trap-corrections are applied are now generated from the 'best 7 columns' from the ^{55}Fe corner source closest to the readout node (see Section B.3).
- Updated PC charge trap offset tables measured using the Si-Kα line from the Tycho calibration observations taken in 2019 August − December, applied from 2019-Jul-15. The trap locations and depths were estimated using a new technique described in Section C.1.
- Updated modelling of the energy dependence of the PC mode trap corrections (based on new observations of SNR E0102 at low energies ($\lesssim 1\,\mathrm{keV}$) and Tycho at higher energies ($\gtrsim 1\,\mathrm{keV}$)).
- Updates to the grade dependent trap-offset scaling factors for the PC mode trap corrections (see Section C.1).
- Updated WT charge trap offset tables created from measurements of the Si-Kα line from the Cas A calibration observations taken from 2019 September, applied from 2018-Jul-15 (see Section C.2).
- Updated modelling of the energy dependence of the WT mode trap corrections (based on new observations of the SNRs E0102, N132D at low energies ($\lesssim 1\,\mathrm{keV}$) and Cas A at higher energies ($\gtrsim 1\,\mathrm{keV}$)).

4 Limitations

The known limitations associated with the gain calibration are described below.

- The accuracy of the trap mapping measurements in PC mode data is dependent on the statistics of the reference Si-Kα line and only traps with a depth greater than $\sim 20\,\mathrm{eV}$ can be reliably identified.
- With the current release we have improved the accuracy of the trap positions in PC mode by merging 5 epochs worth of Tycho data (totalling 1.7 Ms). The greatest fraction of observations, hence the highest statistics, occur in the central regions of the detector, leaving lower statistics outside the central $\sim 200 \times 400$ pixels. The trap mapping analysis in regions with lower statistics only allows the determination of the trap location with an accuracy of ~ 5 pixels.
- The 1D nature of the WT mode readout means traps are not mapped individually and only the cumulative energy offsets of fixed segments along the columns are measured and corrected.
- In datasets affected by scattered light from the sunlit Earth (Bright Earth contamination), optical photons can fill the charge traps and cause spectral shifts to higher energies; in

the worst cases, when observations are taken with CCD temperatures above -55 C, shifts in the energy lines up to ~ 50 eV have been measured. With a change in observation strategy (in 2016), and new guidelines to limit the temperature range, we have minimised these effects, but it is not possible to completely avoid them.

- In between releases of updated gain files new traps caused by radiation damage might develop that can cause shifts in the measured energies that depend on the observed source positions on the detector.
- The gain correction software XRTCALCPI interpolates the gain coefficients between three temperatures. These were originally taken to be -75C, -61.5C and -48C, chosen to match the spread in temperatures seen from the corner source calibration data obtained in $\sim 2008 - 2012$. However, due to spacecraft operational constraints, the majority of observations are now performed over a much narrower range in CCD temperatures — e.g. in 2017 the median temperature was -58.7C, with 90 per cent of observations occurring between -63C to -54C. The three temperatures were changed to -70C, -60C and -50C from 2018-May-31 to reflect this, though this still involves extrapolating the gain coefficients (and trap depths) below -65C and above -52.5C. Occasionally, observations will be taken outside the temperature range covered by the calibration data and can suffer from extrapolation uncertainties, leading to energy scale offsets.

Because of the above limitations and the pixel-specific nature of the distribution of traps on the detector, a general description of the accuracy of the XRT energy scale for the gain file calibration release is not straight-forward. We estimate the accuracy by fitting short observations of the Cas A SNR taken months after the trap-mapping calibration epochs, using a model derived from XMM data. When the line energies are left as free parameters, differences of less than ~ 20 eV from the XMM values are measured in the PC spectrum, while in WT mode the differences can be higher, up to ~ 50 eV at Fe-Kα.

The Leicester calibration team maintains an *XRT Digest* page at the UKSSDC, available at www.swift.ac.uk/analysis/xrt/digest_cal.php, with up-to-date information on the XRT calibration status and the known issues.

APPENDIX

A Gain and CTI coefficients

A.1 Introduction

The charge transfer efficiency (CTE) is defined as the fractional charge lost per pixel during the charge transfer process. So after N transfers the remaining charge Q is

$$Q = Q_o(CTE)^N \tag{A.1}$$

where Q_o is the initial charge. Or in terms of charge transfer inefficiency $CTI = 1 - CTE$ this is just

$$Q = Q_o(1 - CTI)^N \tag{A.2}$$

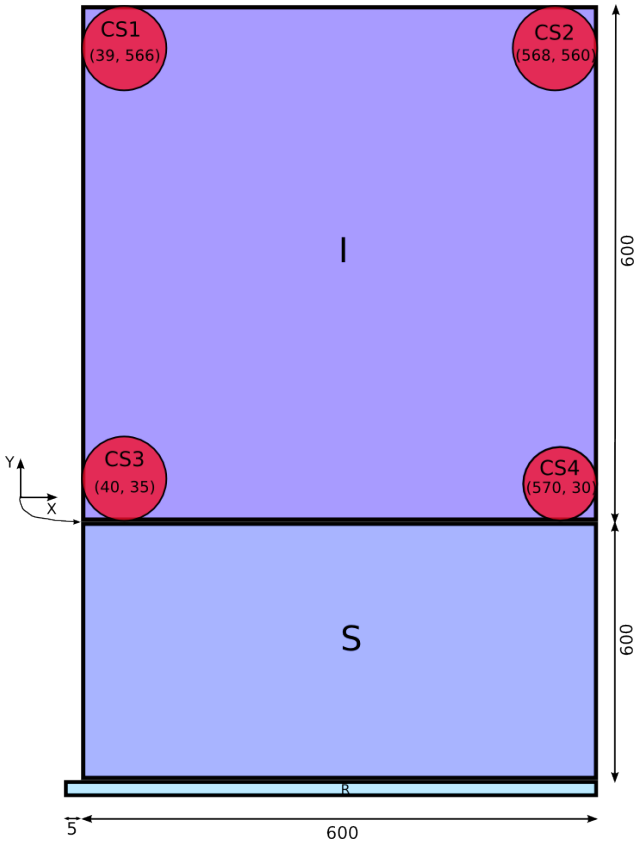

Figure A.1: Schematic of the *Swift*-XRT CCD22 identifying the imaging (I) and frame-store (S) sections, the readout register (R), and the ^{55}Fe corner sources (CS1, ..., CS4). Charged is clocked in the parallel direction (Y), through both the imaging and frame-store sections, which have charge transfer inefficiencies $CTI_{p,i}$ and $CTI_{p,f}$, respectively, and in the serial direction through the readout register with CTI_s.

A.2 Event energy measured in the SWIFT-XRT CCD22

A schematic representation of the *Swift*-XRT CCD22 is showed in figure A.1. When an incident X-ray of energy E is registered as an event at a detector position (X, Y) in the image section it suffers charge loss from Y transfers in the parallel direction through the imaging section, from $Y_S = 600$ transfers in the parallel direction through the frame-store section and from $X + 5$ transfers in the serial direction through the readout register (+5 as there are 5 additional pixels at the end of the readout register). CTI values differ in the parallel and serial direction because of the different transfer times and pixel sizes. In order to describe the total charge lost effectively we need separate CTI coefficients for the parallel transfer losses incurred in the image and frame-store sections ($CTI_{p,i}$ and $CTI_{p,f}$, respectively, as the physical volume of the pixels is smaller in the latter compared with the former) and another for the serial transfer losses (CTI_s).

The event is registered by the ADC as a pulse-height analysed digital number D (i.e. the PHA value) according to the following:

$$D = \frac{E}{A}(1 - CTI_{p,i})^{Y}(1 - CTI_{p,f})^{Y_S}(1 - CTI_s)^{(X+5)} \tag{A.3}$$

Or rearranging slightly, this becomes

$$\begin{aligned} D &= E\left[\frac{(1 - CTI_{p,f})^{Y_S}(1 - CTI_s)^5}{A}\right](1 - CTI_{p,i})^{Y}(1 - CTI_s)^{X} \\ &= \frac{E}{A'}(1 - CTI_{p,i})^{Y}(1 - CTI_s)^{X} \end{aligned} \tag{A.4}$$

where $A' = A/((1 - CTI_{p,f})^{Y_S}(1 - CTI_s)^5)$ is the system gain.

A.3 CTI coefficients

The CCD imaging area is illuminated in its corners by four radioactive ^{55}Fe pellets for calibration purposes, known as the corner sources CS1 ... CS4 (see figure A.1). The parallel CTI can be determined from CS3 and CS1 by using equation A.4 to construct the ratio $(D_3 - D_1)/D_3$, where D_n are the measured ^{55}Fe central energies (in DN) for source $n = 1 \ldots 4$, which is

$$\begin{aligned} \frac{D_3 - D_1}{D_3} &= \frac{(1 - CTI_{p,i})^{Y_3}(1 - CTI_s)^{X_3} - (1 - CTI_{p,i})^{Y_1}(1 - CTI_s)^{X_1}}{(1 - CTI_{p,i})^{Y_3}(1 - CTI_s)^{X_3}} \\ &= 1 - (1 - CTI_{p,i})^{(Y_1 - Y_3)}(1 - CTI_s)^{(X_1 - X_3)} \quad \text{(A.5)} \\ &= 1 - (1 - CTI_{p,i})^{(Y_1 - Y_3)} \quad \text{(A.6)} \end{aligned}$$

where equation A.6 is a simplification assuming $X_1 \approx X_3$ for transfers dominating in the parallel direction (i.e. $Y_1 - Y_3 \gg X_1 - X_3$). Rearranging we find

$$CTI_{p,i} = 1 - \left(\frac{D_1}{D_3}\right)^{1/(Y_1 - Y_3)} \quad \text{(A.7)}$$

We can make use of the small number approximation (i.e. $(1 + x)^n \approx 1 + nx$) so equation A.6 becomes

$$\frac{D_3 - D_1}{D_3} = (Y_1 - Y_3)CTI_{p,i}.$$

That is, the parallel CTI is

$$CTI_{p,i} = \frac{D_3 - D_1}{D_3(Y_1 - Y_3)} \quad \text{(A.8)}$$

A similar equation can be derived for the parallel CTI derived from CS4 and CS2.

Likewise, the serial CTI can be shown to be

$$\begin{aligned} CTI_s &= 1 - \left(\frac{D_4}{D_3}\right)^{1/(X_4 - X_3)} \quad \text{(A.9)} \\ &= \frac{D_3 - D_4}{D_3(X_4 - X_3)} \quad \text{(A.10)} \end{aligned}$$

A.4 Gain coefficient

We can obtain the gain A' from CS3, which is the corner source closest to the output amplifier,

$$A' = \frac{E_{^{55}\mathrm{Fe}}}{D_3}(1 - CTI_{p,i})^{Y_3}(1 - CTI_s)^{X_3} \quad \text{(A.11)}$$

where $E_{^{55}\mathrm{Fe}} = 5895.45\,\mathrm{eV}$, $X_3 = 40$ and $Y_3 = 35$. Note the term $(1 - CTI_{p,i})^{Y_3}(1 - CTI_s)^{X_3}$ provides a small correction to the simple gain estimate of $E_{^{55}\mathrm{Fe}}/D_3$ and ensures the event energy is calculated relative to the origin $(0, 0)$ of the imaging section of the CCD.

A.5 Comparison with the CALDB gain file

The CALDB gain file initially defined the PHA channel to PI channel conversion as

$$PI \times G = PHA\,(GC0 + X \times GC1 + Y \times GC2) + GC3 + X \times GC4 + Y \times GC5 \qquad \text{(A.12)}$$

where GCn are the gain file coefficients (which are interpolated over time and CCD temperature), and $G = 10\,\mathrm{eV}$ is the nominal gain.

Equation A.4 can be rearranged to give the event energy from the measured DN value, assuming the CTI coefficients are known,

$$E = A'\,D\,(1 - CTI_{p,i})^{-Y}\,(1 - CTI_s)^{-X}. \qquad \text{(A.13)}$$

Note, this is the exact form of the equation required to reconstruct the event energy from the measure DN value, knowing the gain (A') and CTI values.

This equation can be made to resemble the CALDB formulation using the small value approximation expansion:

$$\begin{aligned} E &= A'\,D\,(1 + Y\,CTI_{p,i})\,(1 + X\,CTI_s) \\ &= A'\,D\,(1 + X\,CTI_s + Y\,CTI_{p,i} + X\,Y\,CTI_s\,CTI_{p,i}) \end{aligned}$$

and dropping the last (negligibly small) term to give

$$\begin{aligned} E &= A'\,D\,(1 + X\,CTI_s + Y\,CTI_{p,i}) \\ &= D\,\{A' + X\,(A'\,CTI_s) + Y\,(A'\,CTI_{p,i})\}. \end{aligned} \qquad \text{(A.14)}$$

By comparison with equation A.12, we see that

$$\begin{aligned} GC0 &= A' \\ GC1 &= A'\,CTI_s \\ GC2 &= A'\,CTI_{p,i} \end{aligned} \qquad \text{(A.15)}$$

In practise, CTI_s is estimated from corner sources CS3–CS4, while $CTI_{p,i}$ is estimated as the average parallel CTI from corner sources CS1–CS3 and CS2–CS4.

The term $GC3$ in equation A.12 represents an offset (in eV) associated with the readout electronics.

A.6 CTI coefficients' energy dependence

Laboratory experiments and various X-ray missions (e.g. Chandra, Suzaku) indicate that CTI is energy dependent. We choose to implement an energy dependent CTI correction as a broken power law with index β_1 and β_2 below and above the break energy:

$$\begin{aligned} CTI(E) &= CTI(E_{^{55}\mathrm{Fe}}) \left(\frac{E}{E_{^{55}\mathrm{Fe}}}\right)^{-\beta_1} \qquad (E \le E_{^{55}\mathrm{Fe}}) \\ &= CTI(E_{^{55}\mathrm{Fe}}) \left(\frac{E}{E_{^{55}\mathrm{Fe}}}\right)^{-\beta_2} \qquad (E > E_{^{55}\mathrm{Fe}}) \end{aligned} \qquad \text{(A.16)}$$

with $E_{^{55}\mathrm{Fe}} = 5.895\,\mathrm{keV}$ and $\beta > 0$.

The CTI energy dependence parameters in the CALDB gain files are labelled as BETA1, BETA2 and E_CTI.

A.7 Trap correction coefficients

Once the formation of deep traps became apparent on the CCD, we decided to implement trap corrections by including an additional offset term to equation A.12:

$$PI \times G = PHA\,(GC0 + X \times GC1 + Y \times GC2) + GC3 + X \times GC4 + Y \times GC5 + OFFSET \quad \text{(A.17)}$$

(see Pagani et al. 2011). The OFFSET coefficient is added to the $PI \times G$ values of events detected at specific CCD locations affected by charge traps. In the gain files, the trap positions are identified by RAWX, RAWY and YEXTENT, so that the OFFSET PI value is added to events along the CCD column at RAWX between rows RAWY and RAWY + YEXTENT.

The trap offset energy dependence is modelled with a broken power law, with the break at the reference energy of 1.856 keV (the energy of the Si-Kα line of the Tycho SNR):

$$\begin{aligned} OFFSET(E) &= OFFSET(E_{break}) \left(\frac{E}{E_{break}}\right)^{\alpha_1} && (E \le E_{break}) \\ &= OFFSET(E_{break}) \left(\frac{E}{E_{break}}\right)^{\alpha_2} && (E > E_{break}) \end{aligned} \quad \text{(A.18)}$$

The trap-offsets energy dependence parameters are labelled as ALPHA1, ALPHA2 and EBREAK in the CALDB gain files. The gain and CTI coefficients, as well as the energy dependence parameters used by the software to compute the trap-corrected event energy, are identified as GC0_TRAP, GC1_TRAP, GC2_TRAP, GC3_TRAP, GC4_TRAP, GC5_TRAP, BETA1_TRAP, BETA2_TRAP and E_CTI_TRAP.

B Gain and CTI measurements

The gain and CTI coefficients are estimated from the corner source data. A first set of coefficients are derived using the entire corner source dataset, which characterises the CCD response when trap corrections are not applied, to give the PI_NOM energy scale (equation A.12). A second set of coefficients, derived from corner source data least affected by traps, models the gain and CTI of the trap-corrected PI energy scale (equation A.17). For both derivations, the same procedure is applied and is described below.

B.1 Corner source data analysis

The PC mode corner source event data are extracted from the incoming, unfiltered XRT event datasets on a per OBSID basis at the HEASARC *Swift* data-centre and stored in a directory structure which is arranged by calendar month for ease of use. The corner source event files are

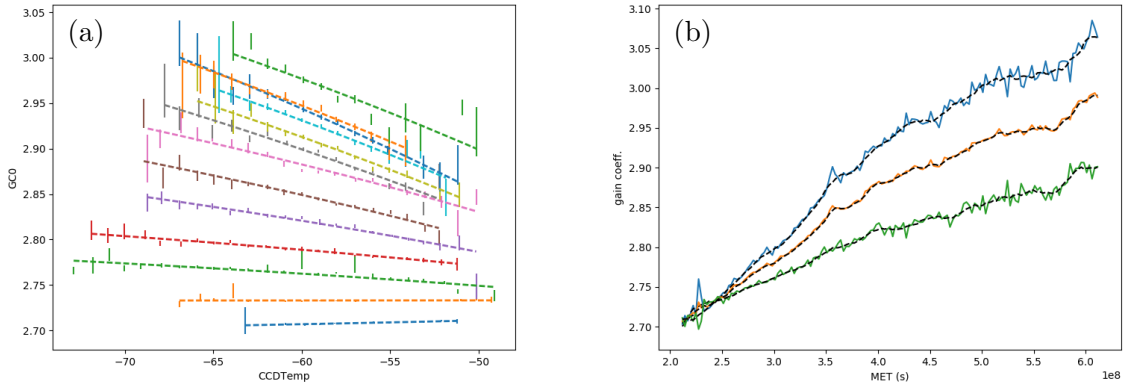

Figure B.1: *Swift*-XRT PC mode gain measurements for the PI_NOM energy scale. The left panel (a) shows the gain coefficient (GC0) versus CCD temperature, plotted yearly, starting from 2007-Sep at the bottom. The measurements are fit with a powerlaw to characterise the temperature dependence of GC0 in each month. The temporal dependence of the gain coefficient is shown in the right panel (b) at CCD temperatures of −70, −60 and −50°C, running from 2007-Sep-05 to 2020-May-31. The black dashed curves in the right-hand panel shows the results after smoothing using a running mean length average over 4 month intervals.

initially processed by the task XRTPCBIAS, which applies temporal and spatial dependent bias corrections to the event 3×3 $PHAS$ values to help counter temperature and/or bright-Earth induced variations in the bias subtraction as the data are accumulated. Hot pixels are then flagged for removal and the 3×3 event islands are assigned a grade and PHA value, before the event files are merged into a single file for that month. Each event is then also tagged with the CCD temperature at the time of the event, interpolated from values in the XRT HK file.

For each month, grade 0 spectra are extracted in 1°C temperature bins. The spectra are then fit around the ^{55}Fe line with the following asymmetric Gaussian function:

$$\begin{aligned} G(x) &= N \exp\left(-0.5\left(\frac{x-x_c}{\sigma_1}\right)^2\right) \qquad (x < x_c) \\ &= N \exp\left(-0.5\left(\frac{x-x_c}{\sigma_2}\right)^2\right) \qquad (x > x_c) \end{aligned}$$

where x_c is the line centre, σ_1 the line width for $x < x_c$, σ_2 the line width for $x > x_c$, and N the normalisation. This models the line profile better and returns more accurate line centroids than a simple Gaussian, as the effect of CTI is to broaden the low energy line wing significantly more than the high energy line wing (Godet et al. 2009, A&A, 494, 775). The centroids are then converted to gain and parallel/serial CTI coefficients following equationA.15.

B.2 Gain and CTI coefficients for non trap-corrected spectra

Figure B.1 shows how the gain coefficient (GC0), estimated from the Gaussian centroids measured from all columns contained in CS3 (i.e., the corner source closest to the readout amplifier), changes with time and temperature from 2007-Sep-05 to 2019-May-31.

For each monthly dataset, a powerlaw is fit to parametrise the observed GC0 versus CCD

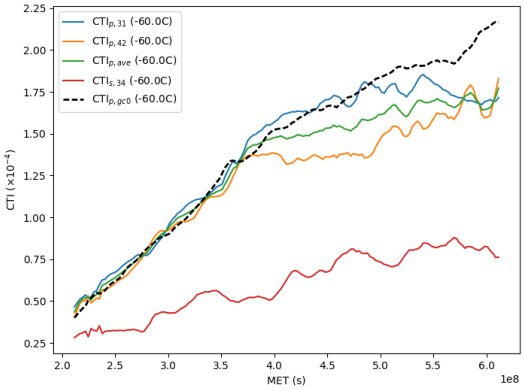

Figure B.2: *Swift*-XRT PC mode CTI at −60°C for the PI_NOM energy scale. The blue and orange curves show the parallel CTI calculated from corner sources $3-1$ and $4-2$, respectively, while the green curve is their average. The red curve shows the serial CTI estimated from corner sources $3-4$. For comparison, the black dashed curve shows the parallel CTI estimated from the change in gain coefficient GC0 from equation A.11.

temperature dependence. The best fit model is then used to estimate GC0 at three temperatures of −70, −60 and −50°C for inclusion in the gain file.

We note that the monthly CCD temperature variations were more pronounced ten years ago than they are today. For example, in 2008, the $10\% - 90\%$ c.d.f. range was ~ 10°C, whereas in 2018 it was ~ 5°C. The shorter temperature baselines can introduce month-to-month variations in the predicted GC0 estimate at −70°C and −50°C. These variations were averaged out by calculating a moving average with running mean length of 4 months.

Figure B.2 shows the temporal behaviour of the parallel and serial CTI coefficients at a CCD temperature of −60°C. The values are converted to gain file coefficients GC1 and GC2 by multiplying by GC0 (see equationA.15). Also included in figure B.2 is an estimate of the parallel CTI coefficient made solely from the change in gain coefficient through equation A.11, which tracks the parallel CTI evolution in the frame-store section.

A template gain file for non trap-corrected data was tested on various data sets which included the corner source data (PC mode) and the line rich SNRs E0102 and Cas A (both PC and WT mode). The low energy spectrum of SNR E0102, in particular, is sensitive to the presence of residual offsets in the energy scale. This is due to the presence of traps that cause energy offsets of the observed energies.

PC mode calibration observations of E0102 taken from 2007 revealed the need for an additional offset for non trap-corrected spectra. The offset is modelled as a function of time with a linear fit and included in the gain file as the GC3 coefficient.

At present, we have no independent measure of the CTI characterisation in WT mode, so use the PC mode CTI coefficients in the construction of the WT gain file. Like PC mode, we checked the residual offset using observations of E0102. These showed an average offset of 40 eV valid for all epochs and included as the GC3 coefficient in the gain files.

Because the deepest traps were not excluded from the corner source analysis described above, the gain and CTI coefficients are representative of a CCD response without trap corrections applied and are labelled in the gain files as GC0, GC1, GC2 and GC3. Note, these coefficients are only used to produce the *PI_NOM* energy scale for calibration purposes and are no longer used by default by XRTCALCPI when performing the gain correction, as the trap-correction analysis is the preferred approach (see below).

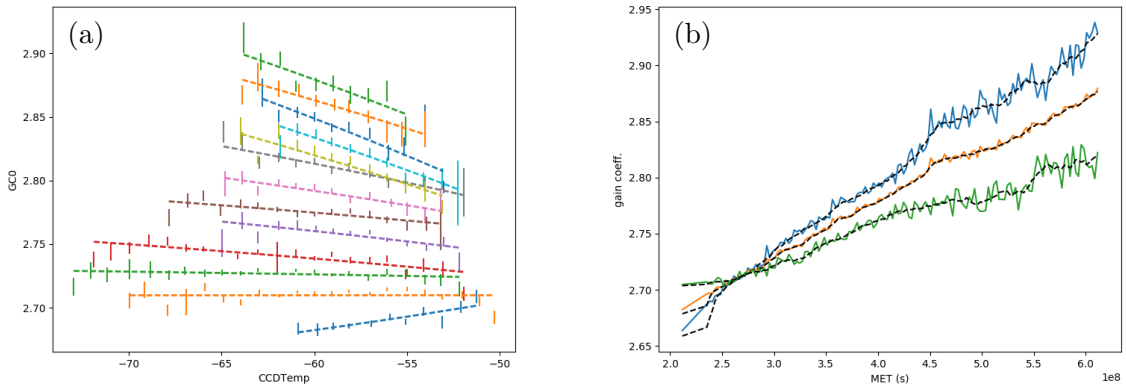

Figure B.3: *Swift*-XRT PC mode gain measurements for trap-corrected data. The left panel (a) shows the gain coefficient (GC0_TRAP) versus CCD temperature, plotted yearly, starting from 2007-Sep at the bottom. The measurements are fit with a powerlaw to characterise the temperature dependence of GC0_TRAP in each month. The temporal dependence of the GC0_TRAP gain coefficient is shown in the right panel (b) at CCD temperatures of −70, −60 and −50°C, running from 2007-Sep-05 to 2020-May-31. The black dashed curves in the right-hand panel shows the results after smoothing using a running mean length of 4 months.

B.3 Gain and CTI coefficients for trap-corrected spectra

When the energy offsets of the deeper traps (> 20 eV) are corrected by the software, the gain is better described by the columns least affected by traps. Therefore, to characterise the gain and the CTI for trap-corrected spectra a subset of the corner source columns are selected.

Prior to this gain file release, the 'best 5 columns' from corner source 3 — i.e. the 5 columns with the highest measured Gaussian centroid, and therefore, least affected by traps — were used in the corner source analysis to create the gain coefficient for the trap-corrected energy scale (for example, see the previous release note, SWIFT-XRT-CALDB-04_v18). However, given the reduction in intensity of the ^{55}Fe radiative source, and the desire to cover as large a CCD temperature range with the best statistic possible, the number of columns considered for the trap-corrected analysis has been increased to 7 starting from this release, applying to data processed after 2018-Aug-01.

The parallel CTI has proven to be more difficult to estimate when considering fewer columns, hence we now use a value predicted from the gain coefficient from the trap free columns through equation A.11. The serial CTI for trap corrected spectra is set to zero in the CALDB files, as global energy offsets for each CCD column are measured and included in the gain file. These gain and parallel CTI coefficients are shown in figures B.3 and B.4.

When trap corrections are applied, the coefficients used by the software task XRTCALPI are called GC0_TRAP, GC1_TRAP, GC2_TRAP and GC3_TRAP in the CALDB gain file.

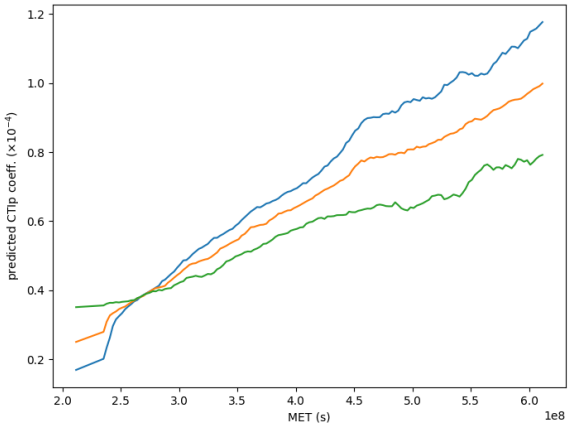

Figure B.4: *Swift*-XRT PC mode parallel CTI for trap-corrected spectra at −70°C (blue), −60°C (red) and −50°C (green), estimated from the change in gain coefficient GC0_TRAP through equation A.11.

C Trap mapping

The extreme radiation environment of low-Earth orbit, particularly when *Swift* transits through the South Atlantic Anomaly, causes degradation to the XRT CCD spectroscopic performance. After $\sim$ 3 years of in-orbit operations, the CTI became more and more dominated by the formation of deep charge traps in individual pixels.

In 2009, we instigated a programme to map the location and depth of the deepest traps in both PC and WT mode. This currently involves performing 15×20 ks observation of the Tycho SNR in PC mode and 6×10 ks observations of the Cas A SNR in WT mode to provide adequate spatial coverage of the CCD. The observations are performed annually, typically in the latter half of the calendar year. In both cases the Si-Kα line is used to measure the depth (and location in PC mode) of the deepest charge traps.

The analysis procedures for both modes are described below.

C.1 Photon Counting Mode

In order to improve the ability of localising individual traps, the last six epochs of Tycho data, from 2014 − 2019, have been merged for a total exposure of 2.1 Ms. The spatial coverage of the merged dataset is shown in detector coordinates in figure C.1 and is representative of the trap-mapping pointing strategy in recent years. On this scale, the Tycho SNR spans a diameter of approximately 200 XRT pixels (or 7.85 arcmin). The highest density of Tycho pointings are made near the centre of the CCD, where 3×20 ks pointings cover the central 200×400 pixels, to coincide with the area where the majority of XRT science observations take place. These are surrounded by another 4×20 ks pointings (at detector positions $200, 200$; $200, 400$; $400, 400$, $400, 200$). Finally, a further 8×20 ks pointings are made with the SNR placed $\sim$ 100 pixels inside from the edges of the CCD.

The procedure for localising the traps and measuring their depths to produce a gain file suitable for applying trap corrections to XRT data is as follows:

1. Process the merged dataset with a gain file containing GC0_TRAP estimated from the

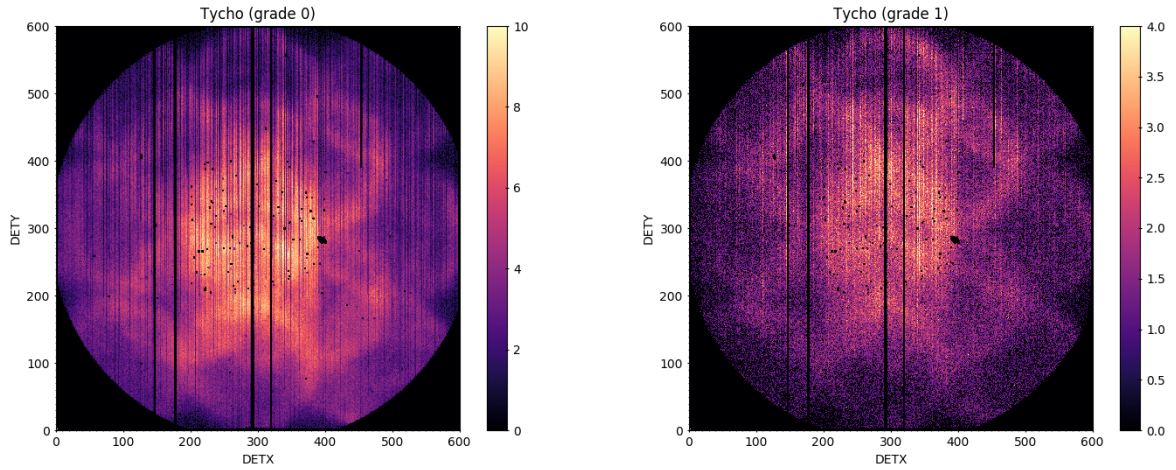

Figure C.1: Merged PC mode data of the Tycho SNR from 2014 − 2019 (exposure 2.1 Ms) showing the spatial coverage of the trap mapping observations. The left panel shows grade 0 (i.e. single pixel) events and the right panel grade 1 (i.e. vertically up-split) events. Note the reduced intensity vertical striations in some columns in grade 0, which appear as corresponding enhanced intensity striations in grade 1, are caused by grade migration as the deepest traps release charge into trailing pixels when the CCD is clocked out in the parallel direction.

best 7 columns and GC2_TRAP from the GC0_TRAP evolution, but with zeroed trap depths — i.e. no trap corrections are applied

2. For each detector column, DETX
   (a) Step through DETY
      i. Accumulate a minimum of 100 counts (from PI 100–220) up the column from current DETY
      ii. Fit for the Si-Kα centroid using the asymmetric Gaussian function.
   (b) Estimate trap locations (i.e. their starting DETY and YEXTENT) up the column using a Bayesian blocks binning algorithm.
   (c) Calculate trap depths at these locations from the *epoch specific* datasets to account for evolution of the traps with time.
3. Calibrate the global trap energy dependence (that is, the parameters α_1, α_2 from equation A.18) at low energies using the SNR E0102 and Tycho spectrum absorption cut-off and at high energies using the Tycho Fe-Kα line.
4. Measure temperature dependent corrections to the trap-depths from the Si-Kα centroids averaged over the CCD in 1° C bins.
5. Calculate grade dependent trap-depth scaling factors for grades 1 − 12 from the Si-Kα centroids averaged over the CCD.

Figure C.2 shows some example columns from the trap analysis procedure, in which the position up the column (DETY) is plotted against the measured Si-Kα Gaussian centroid. These are representative of the different types of behaviour found in the PC mode data, ranging from deep traps (column DETX = 168), to charge-trap filling following hot-pixels (column 127), to largely trap-free columns (column 494).

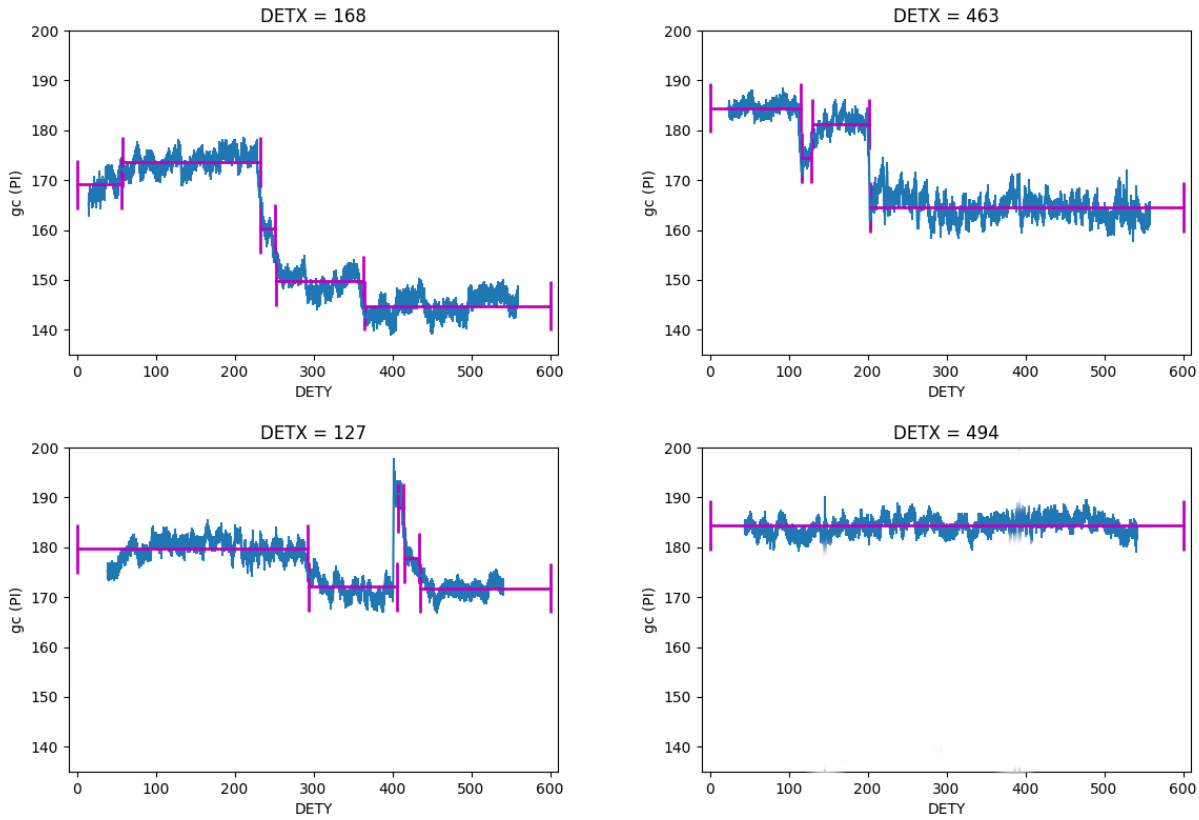

Figure C.2: Example columns from the PC mode trap analysis showing a variety of different behaviour ranging from deep traps (column DETX = 168), a trap followed by recovery (DETX = 463), a high centroid in pixels following a hot-pixel (DETX = 127) and no traps (DETX = 494). The x-axes correspond to the DETY position up the column and the y-axes the Si-Kα centroid (in PI units; the Si-Kα reference energy corresponds to a PI of 185.6). The stepped magenta lines show the position of the traps determined by a Bayesian block binning algorithm.

The trap depths are found to be temperature dependent because, at higher CCD operating temperatures, the associated dark current is higher and fills the traps. This behaviour can be seen, for example, from the corner sources analysis, where the high statistics allow the measurements of depth of individual traps at different temperatures.

The temperature dependence of the measured trap offsets is illustrated in figure C.3, which shows the CCD temperature versus the Si-Kα Gaussian centroid (averaged across the CCD) for the case where a single trap depth is applied at all temperatures (left-hand panel) and after temperature dependent trap offsets are applied (right-hand panel). The offsets are stored at 3 different temperatures in the gain file, which are presently -70° C, -60° C and -50° C, estimated from a powerlaw fit to the observed temperature dependence (the dashed line in figure C.3). The required offset is then found by interpolating as a function of temperature.

New in this release is the identification and implementation of grade dependent trap corrections for PC mode. The left panel of figure C.4 shows CCD averaged Tycho spectra for different grades when the same trap-correction offsets (derived from grade 0 events) are applied, revealing grade dependent effects. For example, grade 1 events — i.e. vertically up-split events — are shifted to higher energies by a grade independent trap-correction as these events contain charge released into the trailing row from that previously trapped in the central event pixel during the readout

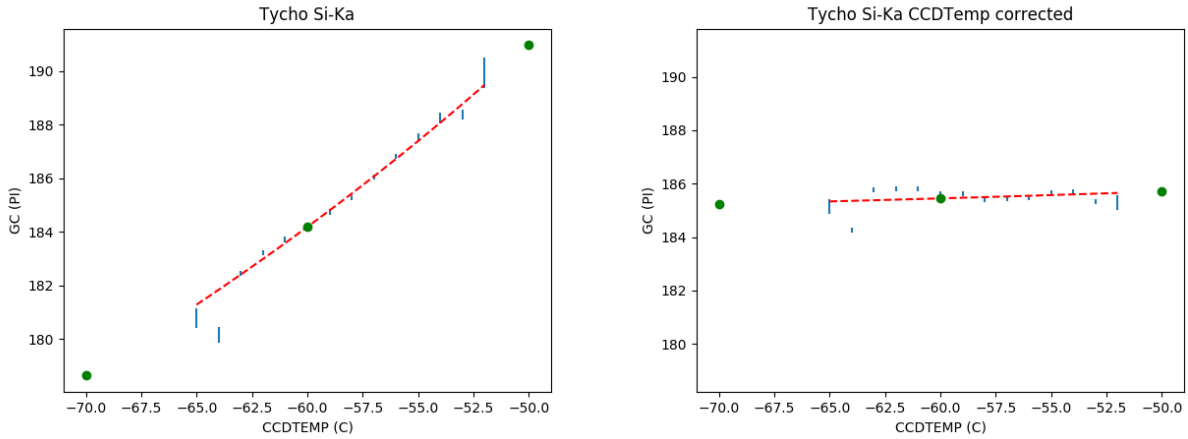

Figure C.3: The PC mode trap correction temperature dependence. The left panel shows the CCD averaged Si-Kα centroids obtained after the same trap corrections are applied at all temperatures. The right panel is the same once temperature dependent trap depths are used. The green circles show the locations of the offsets as predicted at temperatures of -70° C, -60° C and -50° C from the powerlaw fit to the measured centroids (red dashed curve).

Table C.1: PC mode grade dependent trap-offset scaling factors, calculated relative to grade 0 from the Tycho data.

Epoch	Grade									
	0	1	2	3	4	5	6	7	8	$9-12$
2019	1.000	0.451	1.105	0.518	1.017	1.043	1.366	1.366	0.914	0.919
2020	1.000	0.445	1.087	0.550	1.095	0.550	1.200	1.200	0.550	0.815

process. The right panel shows the same spectra once grade dependent scaling factors are taken into account to modify the trap depths as a function of event grade.

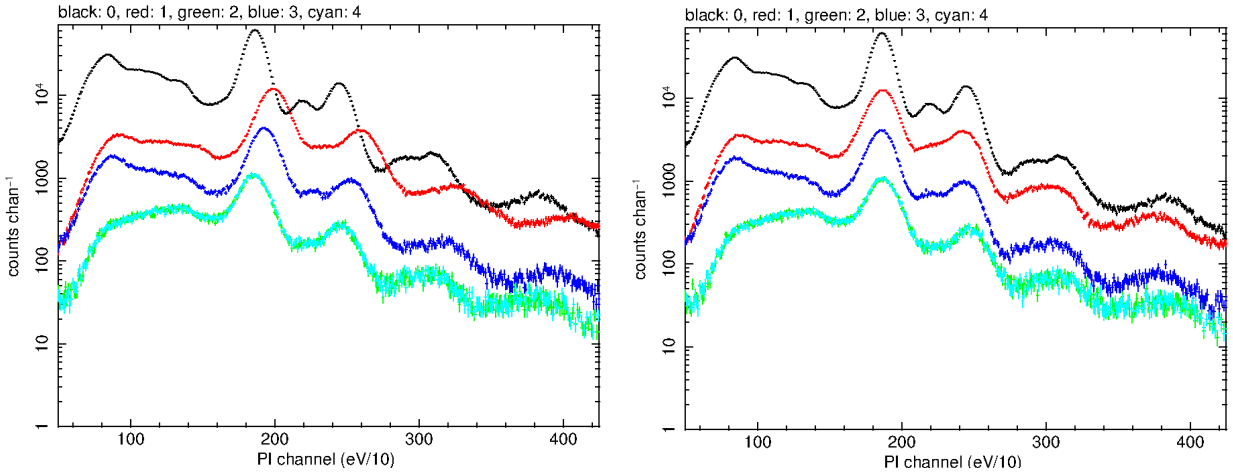

Figure C.4: The PC mode trap correction grade dependence. The left panel shows CCD averaged Tycho spectra obtained as a function of event grade (with black: grade 0, red: 1, green 2, blue 3, cyan 4) with the same trap corrections applied regardless of grade. The right panel is the same once grade dependent scaling factors have been applied to the trap depths.

The requirement for grade dependent trap-corrections in PC mode led to changes to the XRT-

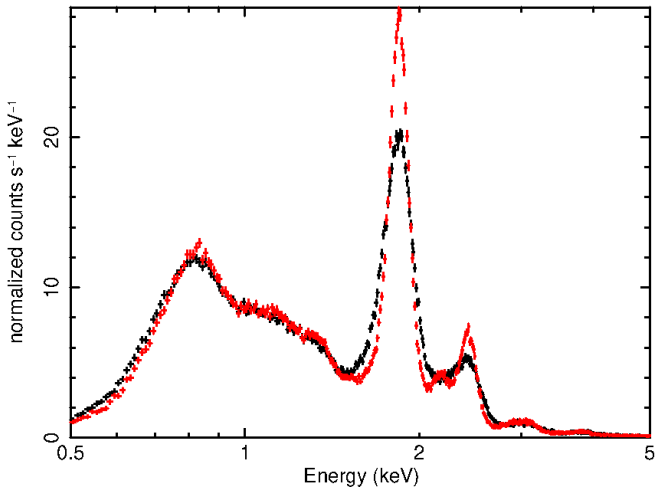

Figure C.5: Comparison of the observed and trap-corrected PC grade $0-12$ spectra of the Tycho SNR taken in 2018-September, showing the improvements obtained when trap corrections are applied. The FWHM of the Si-Kα line is 213 ± 12 eV for the uncorrected spectrum and 143 ± 7 eV for the trap-corrected spectrum.

CALCPI software task and a modification to the CALDB gain file format, with the introduction of a new column (called OFFSET_SCALE) containing the grade dependent trap-offset scaling factors (listed in Table C.1 for PC mode). Because the task uses common code for the other modes (such a WT) this led to the need to reissue the gain files for all modes with the new OFFSET_SCALE column included when the updated software was first released (on 2019-Apr-12), though the scale values were set to 1.0 to disable the grade dependent correction.

The most challenging aspect of the trap-corrected gain file analysis is to simultaneously calibrate both the temperature and energy dependence of the trap corrections, the latter being controlled by the parameters α_1, α_2 from equation A.18. For PC mode data, this was accomplished using the SNR E0102 and Tycho spectrum absorption cut-off at low energies (below ~ 1.0 keV) and the Tycho Fe-Kα line at high energies. The best energy dependence was obtained with $\alpha_1 = 1.0$ and $\alpha_2 = 1.0$.

Figure C.5 shows a comparison of the observed (i.e. non trap-corrected) and trap-corrected spectra obtained from the central Tycho pointing in 2018-September, illustrating the improvements in energy resolution when the trap corrections are applied. The FWHM of the Si-Kα line is 213 ± 12 eV for the uncorrected spectrum and 143 ± 7 eV for the trap-corrected spectrum.

C.2 Windowed Timing Mode

Windowed Timing (WT) mode provides high time resolution (1.78 ms) with 1-D spatial localisation across the central 200 columns of the detector. This makes the WT mode trap analysis conceptually easier as it is not possible to measure both the detector row coordinates and depths of single traps. Furthermore, temperature and grade dependent trap offsets are not required in WT mode because of its continuous and faster charge readout time.

In WT mode, the traps are calibrated using the Cas A SNR, which is positioned at six locations on the detector, for 10 ks each pointing, as shown in figure C.6. This gives two pointings at the bottom [(DETX, DETY) = $(250, 200)$, $(350, 200)$], two in the middle [$(250, 300)$, $(350, 300)$] and two at the top [$(250, 400)$, $(350, 400)$]. The data are initially processed with the trap-free GC0_TRAP and GC2_TRAP coefficients derived for PC mode (see sectionB.3), then global energy offsets from the reference Si-Kα line energy (1.863 keV for Cas A; estimated from an XMM-Newton MOS1 observation) are measured on a column by column basis for each pointing. The SNR has a diameter of ~ 100 XRT pixels (3.9 arcmin), so the offsets are considered to apply

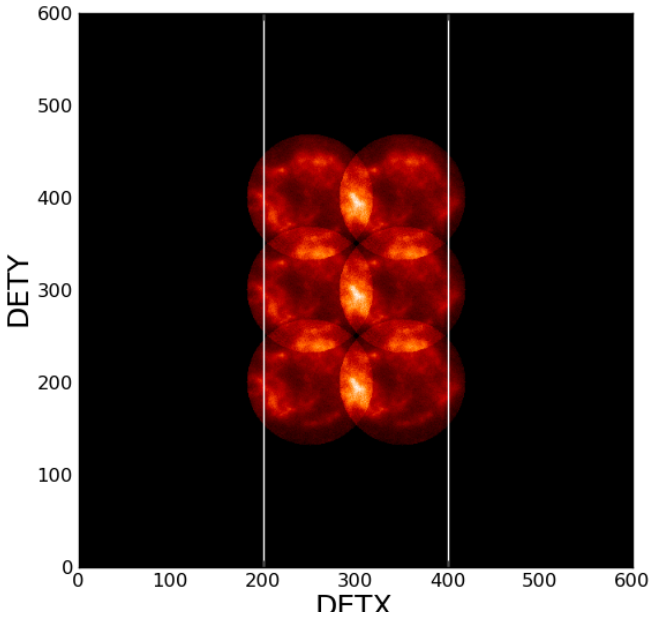

Figure C.6: Illustration showing the location of the six, 10 ks per observation, Cas A pointings (in detector coordinates), used for the WT mode trap analysis.

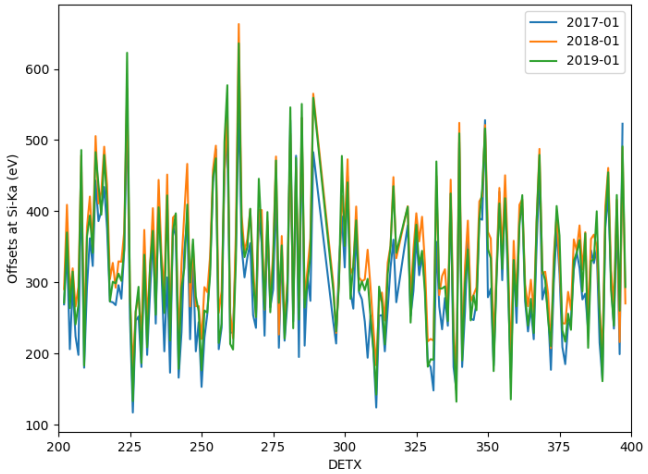

Figure C.7: Column-by-column trap depths measured from the middle Cas A pointings in 2017 (blue), 2018 (orange) and 2019 (green).

over rows DETY $= 251 - 350$ for the middle pointings, $1 - 250$ for the bottom pointings and $351 - 600$ for the top pointings. The trap offsets as measured from $2017 - 2019$ for the middle pointings are shown in figureC.7. Large column-by-column variations are seen, ranging from $\lesssim 150$ eV in the better columns to $\gtrsim 500$ eV in those containing the deepest traps.

Figure C.8 shows a comparison of the observed (i.e. non trap-corrected) and trap-corrected spectra obtained from Cas A in 2018-Dec, illustrating the improvements in energy resolution when the trap corrections are applied. The FWHM of the Si-Kα line is 286 ± 17 eV for the uncorrected spectrum and 192 ± 5 eV for the trap-corrected spectrum. Estimates of the FWHM from previous epochs can be found in the last release note (SWIFT-XRT-CALDB-04_v18).

The trap-correction energy dependence parameters α_1 and α_2 (equation A.18) were calibrated on the SNRs E0102 and N132D, as well as Cas A itself, resulting in $\alpha_1 = 0.875$ and $\alpha_2 = 0.630$. The spectra obtained from E0102 and N132D are illustrated in figure C.9.

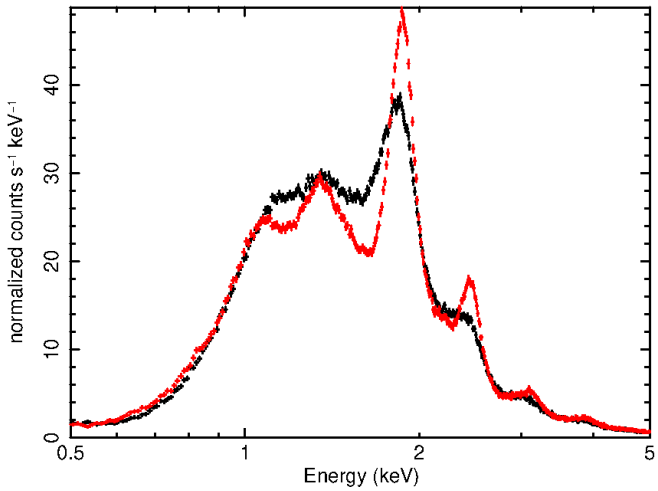

Figure C.8: Comparison of the observed and trap-corrected WT grade 0 spectra of the SNR Cas A taken in 2018-December, showing the improvements obtained when trap corrections are applied. The FWHM of the Si-Kα line is 286 ± 17 eV for the uncorrected spectrum and 192 ± 5 eV for the trap-corrected spectrum.

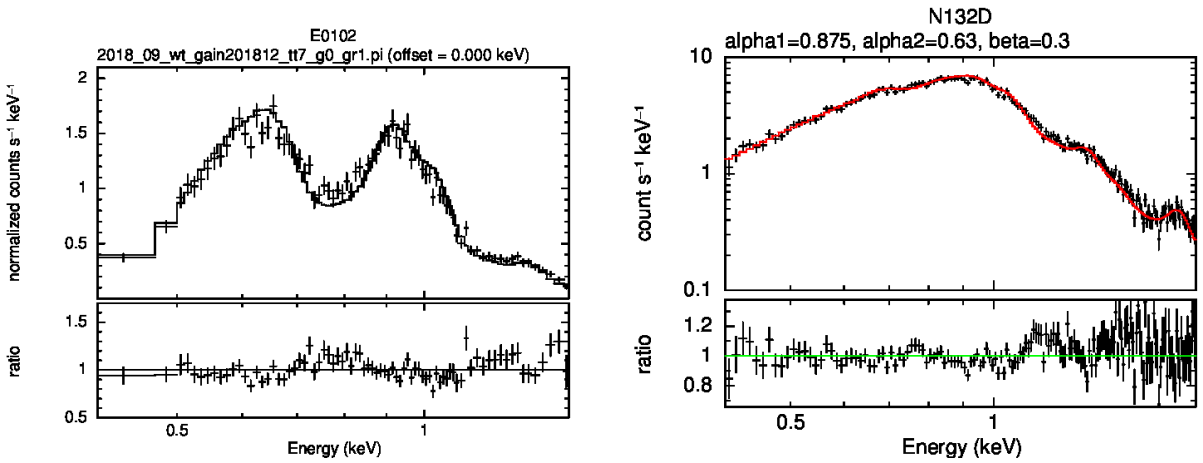

Figure C.9: WT mode spectra of E0102 (left panel) and N132D (right panel), used to calibrate the low E energy scale, fit with their respective IACHEC models.

D Previous Gain File Releases

Table D.1 lists the gain files made available through previous releases of the *Swift*-XRT CALDB. A web page summarising the releases, along with an archive of older release notes, is available from the University of Leicester's UKSSDC *Gain and RMF release summary* page.

Table D.1: Previous gain file releases.

FILENAME	VALID DATE	RELEASE DATE	REVISION
swxpcgain20010101v003.fits	2001-Jan-01	2004-Oct-15	003
swxpdgain20010101v003.fits	2001-Jan-01	2004-Oct-15	003
swxwtgain20010101v003.fits	2001-Jan-01	2004-Oct-15	003
swxpcgain20010101v004.fits	2001-Jan-01	2005-Jan-10	004
swxpdgain20010101v004.fits	2001-Jan-01	2005-Jan-10	004
swxwtgain20010101v004.fits	2001-Jan-01	2005-Jan-10	004
swxpcgain20010101v005.fits	2001-Jan-01	2005-Oct-12	005
swxpdgain20010101v005.fits	2001-Jan-01	2005-Oct-12	005
swxwtgain20010101v005.fits	2001-Jan-01	2005-Oct-12	005
swxpcgain20010101v006.fits	2001-Jan-01	2005-Dec-01	006
swxpdgain20010101v006.fits	2001-Jan-01	2005-Dec-01	006
swxwtgain20010101v006.fits	2001-Jan-01	2005-Dec-01	006
swxpcgains0_20010101v007.fits	2001-Jan-01	2007-Jul-30	007
swxpcgains6_20010101v007.fits	2001-Jan-01	2007-Jul-30	007
swxpdgains0_20010101v007.fits	2001-Jan-01	2007-Jul-30	007
swxwtgains0_20010101v007.fits	2001-Jan-01	2007-Jul-30	007
swxwtgains6_20010101v007.fits	2001-Jan-01	2007-Jul-30	007
swxwtgains0_20010101v008.fits	2001-Jan-01	2008-Apr-21	008
swxwtgains6_20010101v008.fits	2001-Jan-01	2008-Apr-21	008
swxpcgains0_20010101v008.fits	2001-Jan-01	2009-Apr-07	009
swxwtgains0_20010101v009.fits	2001-Jan-01	2009-Apr-07	009
swxpdgains0_20010101v008.fits	2001-Jan-01	2009-Apr-07	009
swxpcgains6_20010101v008.fits	2001-Jan-01	2009-Apr-07	009
swxwtgains6_20010101v009.fits	2001-Jan-01	2009-Apr-07	009
swxpcgains6_20010101v009.fits	2001-Jan-01	2009-Dec-01	009
swxwtgains6_20010101v010.fits	2001-Jan-01	2009-Dec-01	009
swxpcgains6_20010101v010.fits	2001-Jan-01	2011-Jun-07	010
swxwtgains6_20010101v011.fits	2001-Jan-01	2011-Jun-07	010
swxpcgains0_20010101v009.fits	2001-Jan-01	2011-Jun-07	010
swxwtgains0_20010101v010.fits	2001-Jan-01	2011-Jun-07	010
swxpdgains0_20010101v009.fits	2001-Jan-01	2011-Jun-07	010
swxpcgains6_20010101v011.fits	2001-Jan-01	2012-Feb-09	011
swxwtgains6_20010101v012.fits	2001-Jan-01	2012-Feb-09	011
swxpcgains0_20010101v010.fits	2001-Jan-01	2012-Feb-09	011
swxwtgains0_20010101v011.fits	2001-Jan-01	2012-Feb-09	011
swxpdgains0_20010101v010.fits	2001-Jan-01	2012-Feb-09	011
swxpcgains6_20010101v012.fits	2001-Jan-01	2013-Feb-09	012

Table D.1: Previous gain file releases (continued).

FILENAME	VALID DATE	RELEASE DATE	REVISION
swxwtgains6_20010101v013.fits	2001-Jan-01	2013-Feb-09	012
swxpcgains0_20010101v011.fits	2001-Jan-01	2013-Feb-09	012
swxwtgains0_20010101v012.fits	2001-Jan-01	2013-Feb-09	012
swxpcgains6_20010101v013.fits	2001-Jan-01	2013-Dec-20	013
swxwtgains6_20010101v014.fits	2001-Jan-01	2013-Dec-20	013
swxwtgains6_20010101v015.fits	2001-Jan-01	2014-Jul-30	014
swxpcgains6_20010101v014.fits	2001-Jan-01	2015-Aug-03	015
swxwtgains6_20010101v016.fits	2001-Jan-01	2015-Aug-03	015
swxpcgains6_20010101v015.fits	2001-Jan-01	2016-May-10	016
swxwtgains6_20010101v017.fits	2001-Jan-01	2016-May-10	016
swxpcgains6_20010101v016.fits	2001-Jan-01	2017-May-01	017
swxwtgains6_20010101v018.fits	2001-Jan-01	2017-May-01	017
swxpcgains6_20010101v017.fits	2001-Jan-01	2018-Jul-10	018
swxwtgains6_20010101v019.fits	2001-Jan-01	2018-Jul-10	018
swxpcgains0_20010101v012.fits	2001-Jan-01	2019-Apr-12	19
swxwtgains0_20010101v013.fits	2001-Jan-01	2019-Apr-12	19
swxpdgains0_20010101v011.fits	2001-Jan-01	2019-Apr-12	19
swxpcgains6_20010101v018.fits	2001-Jan-01	2019-Apr-12	19
swxwtgains6_20010101v020.fits	2001-Jan-01	2019-Apr-12	19
swxpcgains6_20010101v019.fits	2001-Jan-01	2020-Oct-23	20
swxwtgains6_20010101v021.fits	2001-Jan-01	2020-Oct-23	20

Note, the gain files are named according to the convention

swx**mm**gains**S**_**YYYYMMDD**v0**XX**.fits,

where **mm** identifies the CCD readout mode (either 'pc' for Photon Counting, 'pd' for Photo-Diode, 'wt' for Windowed timing), **sS** the CCD substrate voltage (with **'s0'** referring to substrate voltage 0V and **'s6'** to substrate voltage 6V gain files; the substrate voltage was raised permanently to 6V on 2007-Aug-30 at 14:25UT — i.e. all data taken since then have been taken at 6V), **YYYYMMDD** is the date from which the file is first used and **'XX'** is the version of the gain file for the particular readout mode, substrate voltage and epoch.

The main XRT data processing script, XRTPIPELINE, invokes the gain correction task XRTCALCPI with the appropriate gain file (i.e. mode and epoch) when event files are processed.

References

Useful references pertaining to XRT calibration are listed below:

Godet, O., Beardmore, A. P., Abbey, A. F., et al. 2007, SPIE, 6686
Godet, O., Beardmore, A. P., Abbey, A. F., et al. 2009, A&A, 494, 775
Pagani, C., Beardmore, A. P., Abbey, A. F., et al. 2011, A&A, 534, A20
Beardmore, A. P., et al. 2013, SWIFT-XRT-CALDB-09_v18, Substrate voltage 0V and initial 6V RMF/ARF release note
Beardmore, A. P., et al. 2014, SWIFT-XRT-CALDB-09_v19, Epoch dependent substrate voltage 6V RMFs release
Beardmore, A. P., et al. 2018, SWIFT-XRT-CALDB-04_v18, 2018-Jul-10 gain files update